Resonant Stimulated Photorefractive Scattering

Jingliang Liu,[1,2] Thomas Stace,[3] Jian Dai,[1] Kun Xu,[1] Andre Luiten,[2,*] and Fred Baynes[2]
[1]State Key Laboratory of Information Photonics and Optical Communications, Beijing University of Posts and Telecommunications, Beijing 100876, China
[2]Institute for Photonics and Advanced Sensing (IPAS) and The School of Physical Sciences, The University of Adelaide, Adelaide 5005, Australia
[3]ARC Centre of Excellence for Engineered Quantum Systems (EQUS), School of Mathematics and Physics, University of Queensland, Brisbane 4072, Australia

(Received 4 February 2020; revised 20 March 2021; accepted 9 June 2021; published 16 July 2021)

We present the first observations, and a complete theoretical explanation, of stimulated photorefractive scattering in a high- Q crystalline cavity. The standing-wave light field in the cavity induces an ultranarrow and long-lived Bragg grating through the photorefractive effect. The spatial phase of the grating is automatically matched to that of the standing wave. The scattering from the grating strengthens the standing wave, which then further reinforces the grating itself. Eventually, the mode is seen to split into a doublet, thereby disrupting the usual strict periodicity of the mode spectrum.

DOI: 10.1103/PhysRevLett.127.033902

Stimulated scattering processes are a fundamental aspect of nonlinear optics. In microresonators, the small size, long photon lifetime, and high optical intensities allow stimulated scattering processes at relatively low powers and have thus yielded breakthrough new applications in sensing [1–4], quantum systems [5–8], and photonics [9–14]. In the stimulated photorefractive scattering (SPS) case, a standing-wave light field generates a photorefractive grating, which increases the amount of coherent backscattering, thereby increasing the strength of the standing wave. The amplified standing wave then, in turn, stimulates a further strengthening of the SPS grating. This self-reinforcing interaction produces a self-sustaining grating in which the spatial phase of the grating is matched to that of the incident light field itself.

In bulk crystals, the standard photorefractive effect has been studied in the past as a method of optical data storage [15], while SPS has been used as a basis for optical phase conjugation [16]. The conventional photorefractive effect has also been observed previously in microresonators [17–19]. However, in this Letter we present the first report of the complex, and potentially useful, impact of SPS inside a high-Q resonator. Our observations open a new avenue to augment the important prior work on analogous stimulated Brillouin scattering (SBS) and stimulated Raman scattering (SRS) effects in microresonators. Those effects have been used to deliver gyroscopes [4], slow light generation [8], lasers [9,10], and microwave photonic technology [11,12]. There has been parallel work on the use of mode splitting to demonstrate single-particle sensing [1,20], discovering wave chaos [21], allowing the breaking of time-reversal symmetry [22], creating synchronization between oscillators [23], as well as creating photonic molecules [13].

In these experiments, we use a z-cut undoped lithium niobate (LN) microresonator with a diameter of 9.5 mm, a thickness of 1 mm, and a Q factor of 3.4×10^8 that was cut and polished in house from a commercially available LN crystalline blank (see Fig. 1). A 1560-nm laser beam is evanescently coupled to the microresonator with a prism to excite highly confined whispering gallery modes. We use a circulator to allow observation of both the transmitted and backscattering light as shown in Fig. 2(b) (red curve). The laser is frequency locked to the blue-shifted wing of a

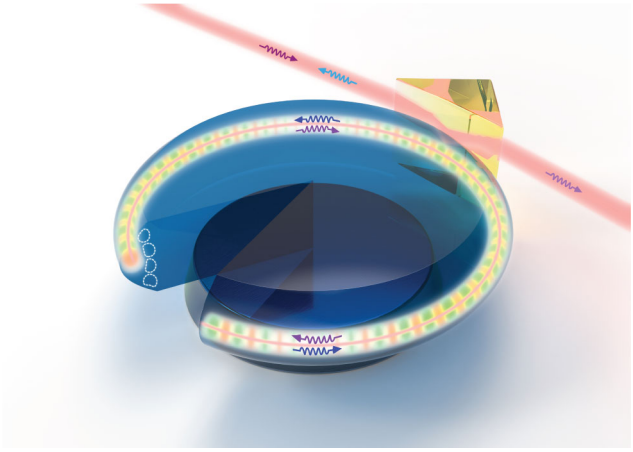

FIG. 1. Diagram of SPS in a lithium niobate microresonator excited by an external laser. Light is coupled via a closely spaced prism and the incident field (purple arrow in laser beam) produces a forward-traveling wave in the resonator (purple arrow in resonator). Backscattered light from the induced SPS grating is contained within the same spatial mode and produces a standing wave inside the resonator (dark blue) that reinforces the SPS grating.

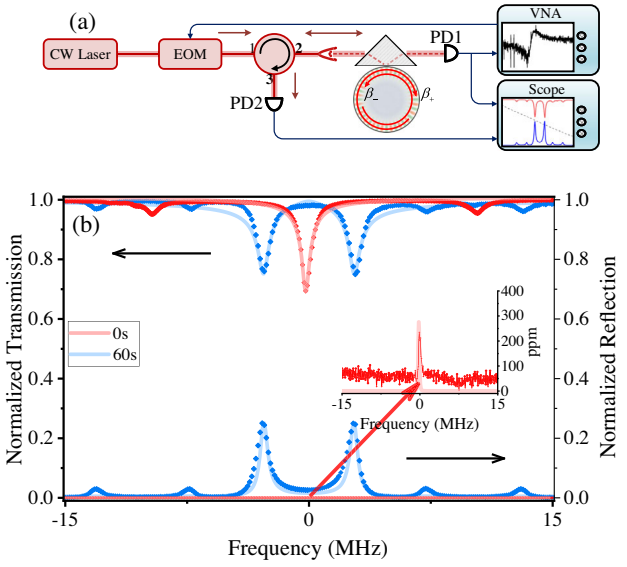

FIG. 2. Experimental layout and measurements. (a) The experimental layout: a tunable laser is coupled to the resonator via a prism coupler, while the transmitted and backscattered power is measured using photodiodes (PD) on the ports of a circulator and the mode spectrum are read from the scope. The splitting process is measured using a vector network analyzer (VNA) while the laser is locked to the higher frequency mode and electro-optically generated sidebands are swept over the lower frequency mode. (b) Experimental measurements of the mode spectrum (dot) and simulations (solid curves) of the resonator transmission (upper) and the backscatter (lower), which is normalized according to the transmission. We show the transmission both under the initial conditions (red) and after 60 s (blue). The insert is the zoomed-in view of the initial backscattering with the same normalization showing the very low level of initial backscatter.

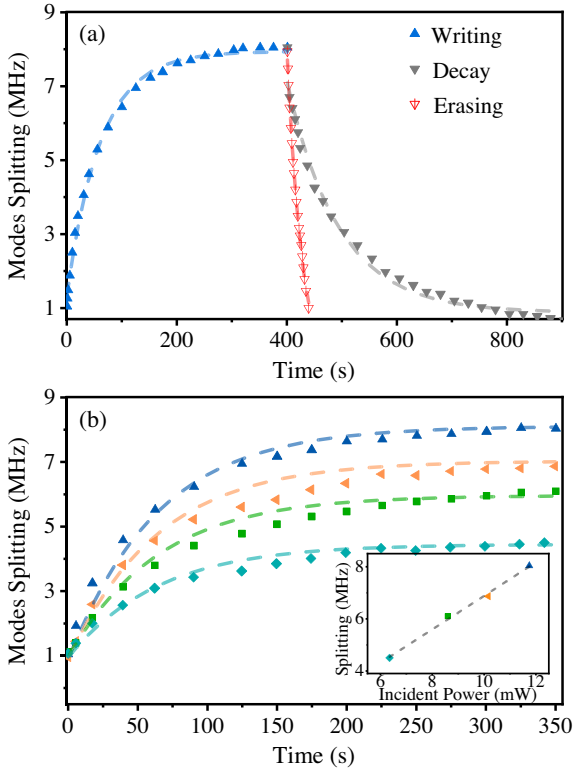

FIG. 3. Dynamic response of SPS in the microresonator. (a) Experimental measurements of the mode splitting during a writing phase (blue dots) and during the decay phase (gray dots) when the laser is extinguished. Both curves can be fit to exponential responses (dashed curves). We also show the response of the cavity during an erasure phase (red dots) when the laser is injected into the other mode of the mode pair. (b) Experimental data (dots) of the mode splitting process for different incident powers, while the dashed curves are the simulation results. Inset: the linear dependence of the splitting on incident power.

high- Q mode using the Pound-Drever-Hall technique [24]. This mode initially exhibited only a small level of backscattering [inset in Fig. 2(b)]. However, once the laser was locked at that frequency location, we see a very rapid increase in the level of backscattering: within ~10 s it was approximately equal in intensity to that of the forward wave. From that point onward, we observe the mode to split into a doublet with a frequency separation between the components that increases over time [blue curves in Figs. 2(b) and 3(a)]. The Q factors of the split modes remain constant throughout the process, implying that the mode-coupling mechanism creates a negligible increase in the resonator losses.

We explain these observations as arising from a self-induced photorefractive grating that couples the forward and backward propagating modes. Scattering associated with inhomogeneities of the resonator generates the initial weak backreflected field [25]. The combination of forward and backward waves can equally be considered as a weak standing wave and strong forward wave. As LN is a photorefractive material [17], the intensity modulation associated with the standing-wave component gives rise to a photorefractive grating with a period equal to half of the wavelength of the incident light. The induced grating then backscatters more light into the backward propagating mode, thus increasing the strength of the standing wave, which then in turn strengthens the photorefractive grating further. Eventually the grating strength is sufficient that the coupling between forward and backward traveling modes exceeds the dissipative coupling, and we then see frequency splitting of the mode.

As the mode splitting increases, the frequency-locked laser automatically tracks the high-frequency wing of the upper member of the doublet (as it was initially locked on the blue wing of the unsplit mode). To obtain the splitting spectrum of the resonator in real time, we use an electro-optic modulator and a vector network analyzer to generate frequency tunable optical sidebands on the locked laser signal. These sidebands are continuously swept over the complete mode doublet and read by the vector network analyzer to obtain the splitting spectrum [26]. The splitting

frequency is seen to undergo an exponential increase to a steady-state value with a large time constant characteristic of the photorefractive effect [27]. Figures 3(a) and 3(b) show the mode splitting as a function of time, demonstrating a time constant of ~60 s independent of the input power. We also note that the stimulated backscattering and mode splitting have a threshold of 600 μW, similar to that previously observed for the normal photorefractive effect in LN microresonators of this Q factor [18]. Figure 3(b) also demonstrates that the asymptotic value of the mode frequency splitting is linearly dependent on power, enabling a high degree of controllability over the mode coupling.

If the pump laser is switched off then the mode splitting is seen to decrease with a time constant of around 90 s, until the two modes coalesce [see Fig. 3(a)]. In a separate experiment, once the mode splitting had reached its maximum value, the laser was locked to the center frequency of the lower frequency component of the mode doublet. This induced a very rapid recombination of modes [red curve in Fig. 3(a)]: the grating was seen to be effectively erased from the resonator by this process with a time constant of ~30 s.

Motivated by the observed splitting, we propose a phenomenological mode-coupling theory that captures the experimental results [28,29]:

$$\frac{d}{dt}\beta_+ = (i2\pi\Delta f - \gamma_R/2)\beta_+ + i\delta_G\beta_-/2 + i\sqrt{\gamma_E}\beta_I, \tag{1}$$

$$\frac{d}{dt}\beta_- = (i2\pi\Delta f - \gamma_R/2)\beta_- + i\delta_G\beta_+/2, \tag{2}$$

where β_+ and β_- are amplitudes of the forward and backward propagating waves, Δf denotes the laser detuning from the resonant mode, β_I is the incident light field, and γ_E represents the coupling coefficient to the prism. The photon loss rate in the resonator is defined as $\gamma_R = \gamma_E + \gamma_0$, where γ_0 is the intrinsic (unloaded) photon scattering loss rate.

The mode coupling between forward and backward modes δ_G arises from both resonator inhomogeneities (material or geometry), as well as from the induced SPS grating. We introduce these phenomenologically via

$$\delta_G(t) = \delta_0 + \xi(1 - e^{-t/\tau_p})|\beta_+^*\beta_-|, \tag{3}$$

where δ_0 is the scattering from static inhomogeneities. The induced grating emerges endogenously from field ionization of space charges that diffuse over a timescale τ_p to generate a local charge density. The resulting static electric field induces the SPS grating via the electro-optic effect. At long times, the SPS grating has an effective depth controlled by material and geometric factors that are incorporated through the coefficient ξ and by the modulation depth of the standing wave $\propto |\beta_+^*\beta_-|$.

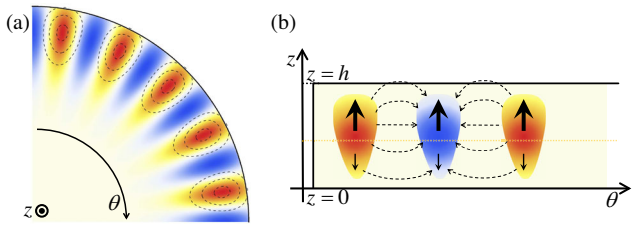

FIG. 4. Diagram for the stable standing-wave mode function (dashed), charge density (color), and electric field lines. (a) Once the photorefractive grating (colored) is generated, the induced grating reflection will help to build the standing waves (dashed) $\beta_\pm = \beta_+ \pm \beta_-$ with different frequencies in azimuthal distribution. (b) The arrows are the charge density in the z direction, and the colored area is the asymmetric distributed refractive index that forms the grating.

In the Supplemental Material [30], we derive the steady-state version of Eq. (3), using a self-consistent, nonlinear mode-coupling theory that accounts for charge diffusion and the electro-optical indicatrix tensor. This derivation provides the microscopic dependence of ξ on material and geometric properties of the resonator. In summary, this analysis considers a spatial mode decomposition that has standing modes around the resonator circumference, illustrated in Fig. 4(a), and then includes a vertical asymmetry for those mode functions (i.e., for reflections about the midplane of the resonator) as illustrated in Fig. 4(b). This asymmetry is parametrized by ζ in the axial mode function $\mathsf{Z}(z) = \sin(\pi z/h) + \zeta\sin(2\pi z/h)$, where $z = 0$ and $z = h$ are the bottom and top surfaces of the resonator, respectively. This analysis demonstrates that the nonlinear coupling constant ξ in Eq. (3) depends on the asymmetry parameter ζ. For perfect midplane reflection symmetry, i.e., when $\zeta = 0$, the resonator mode is even under reflection about $z = h/2$, and under this condition it follows that the resulting electric field due to space charges will be an odd function under reflection. This leads to zero coupling to the induced grating, i.e., ξ vanishes. For small reflection asymmetry, we find $\xi \propto \zeta$.

One significant result of this nonlinear coupling theory is that only one of the components of the mode doublet will produce a self-consistent solution; i.e., only the blue-shifted peak of the doublet is stable, whereas the red-shifted doublet is dynamically unstable, as its standing-wave mode function is not consistent with the induced grating that is produced by charge diffusion from the standing wave itself. This theoretical result is consistent with our observations: to initiate significant SPS, the laser must be locked to the higher frequency component of the doublet as it emerges dynamically. We observe the presence of the lower frequency component if we probe the resonator with a weak beam; however, this secondary mode is not stable: locking the laser to it quickly erases the SPS-induced grating in the microresonator. Naturally, the photorefractive grating in a resonator must be induced by an electric field distribution that is phase matched to the supported modes (Fig. 4).

In Fig. 3(a), we treat ξ and τ_p as fitting parameters. These parameters are then held fixed for the fits in Fig. 3(b), where we then only adjust the relative value of β_I to be in accord with the experimental values. We note excellent agreement between the theory and the experiment.

The periodic modulation of the refractive index created by the stimulated refractive scattering is a form of Bragg grating, and we have derived the underlying parameters of the SPS grating such as the length, depth of index of refraction modulation, and the grating bandwidth [29] in terms of the mode coupling and photon scattering rate:

$$\delta f_G = f_0 \delta_G \sqrt{1 + (2\pi\gamma_R/\delta_G)^2}/2\pi. \tag{4}$$

The grating bandwidth will evolve during the writing process as shown in Fig. 5: at the onset of SPS, the backscattering rate is below the photon loss rate, so the system is in the weak grating regime ($\delta_G < \gamma_R$) [29]. In this regime, the bandwidth is fixed by the grating length, which is the total effective path length of the photons in the resonator, and it is equal to $2\pi\delta f_R$, where δf_R is the resonance bandwidth. The very high Q factor of the LN microresonator gives an effective grating length of 38 m, and using the experimentally derived mode-coupling parameters and Eq. (4), the weak grating has a record narrow bandwidth of 3.6 MHz and a refractive index modulation, $\Delta n = 6.5 \times 10^{-9}$. However, the effective bandwidth of the grating is much narrower than this because it is limited by the resonance bandwidth to a value of 570 kHz.

As the stimulated process continues, the refractive index modulation grows, and the coupling becomes stronger. In the strong grating regime ($\delta_G > \gamma_R$), the scattering is sufficiently strong that the counterpropagating modes have essentially equal power, and the standing wave will achieve the maximum contrast. In this case, there is significant mode splitting and the SPS bandwidth is equal to the mode separation. In this experiment we see a maximum splitting and hence SPS gain bandwidth of 8.8 MHz.

An important aspect of SPS in a microresonator is the highly selective nature of the stimulated scattering. The SPS grating is automatically phase matched to the mode in which it has been excited and, because its bandwidth is much smaller than the intermode spacing there is SPS interaction and backscattering only in a single resonance. In Fig. 6, it can be seen that the SPS grating does not produce mode splitting in the next higher frequency member of the same mode family, i.e., the mode with an azimuthal mode number incremented by 1. We do observe a frequency shift with the same time constant as the excited mode, but there is no mode coupling or splitting. This is consistent with a situation in which there is no spatial phase matching between the grating and this second mode, but where that second mode still samples the change in average refractive index that has been produced by the induced grating.

If we operate the SPS induced grating in the weak grating regime (see Fig. 5) there is a strong backscattering for only a single mode with an effective spectral selectivity equal to the Q factor of 3.4×10^8. This observation opens the

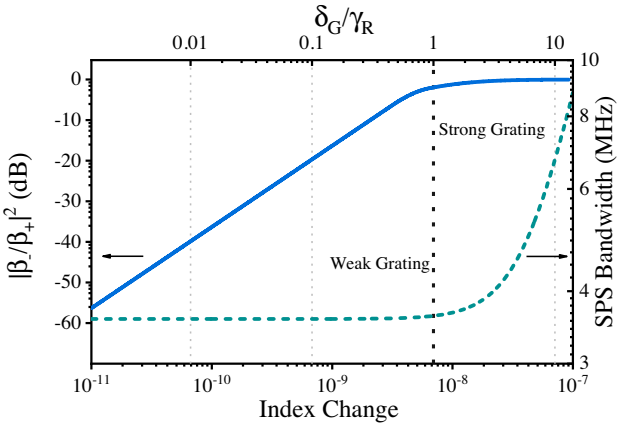

FIG. 5. Evolution of the SPS bandwidth. The lower axis shows the magnitude of the modulation of the refractive index from the SPS grating, while the upper axis is the ratio of the photon and scattering lifetime τ_R/τ_G and this parameter reflects the strength of the mode coupling. On the left axis (blue, solid) is the ratio of the backward to forward traveling waves $|\beta_-/\beta_+|^2$ and on the right axis (teal, dashed) is shown the SPS grating bandwidth. After initiation of SPS, the conditions evolve to the right on this diagram, showing a rapid initial increase in backscattering and then, once this has saturated, we see an increase in the mode splitting. In parallel, we see an initial SPS gain bandwidth of 3.6 MHz, which at the critical point (black dot) is equal to $2\pi\delta f_R$.

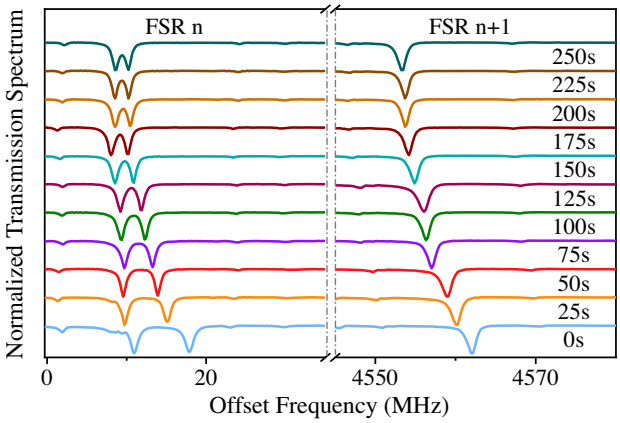

FIG. 6. Effect of SPS on two modes with adjacent angular momentum numbers that are separated by one free spectral range (FSR). The left-hand panel shows the recombination of the mode into which we have injected power to produce a mode splitting. We see the decay of the mode splitting, as well as a shifting of the mean frequency as a result of the decay of the background photorefractive effect. Concurrently, the right-hand side shows the same mode family in the next FSR and in this case the mode shows merely the effect of the decay of the spatially uniform photorefractive effect, but shows no evidence of mode splitting.

possibility for a very high performance optoelectronic oscillator [33] or microwave photonic filter [12] with an exceptionally large tunability into the THz range.

Instead, if we operate the grating in the strong coupling limit, then this opens the possibility to break the conventional uniformity of the mode spectrum of any resonator by modifying the spectrum of a single mode. This "defect" mode could prevent unwanted spontaneous conversion in microresonator-based approaches to coherent single-photon microwave-to-optical conversion [34].

In summary, we report the first observations of stimulated photorefractive scattering (SPS) in a microresonator that gives rise to some surprising and unique phenomena. The requirement for self-consistency between the modes of the resonator and induced SPS grating means that unlike in conventional mode coupling, only one of the resultant doublet peaks is optically stable. The stimulated effect is automatically phase matched and has a lifetime of 60 s, far exceeding the lifetime of other nonlinear effects. We observe a mode splitting that can be up to 15 times larger than the mode bandwidth. Using those observations, we are able to calculate the properties of the underlying SPS grating, showing a grating length of 36 m and a bandwidth of 3.6 MHz, although the filtering effect of the resonator means that it is effectively limited to only 570 kHz.

A. L., F. B. and T. S. wish to thank the South Australian government and the Australian Research Council (Grants No. F00001293, No. FT0991631, No. DP0877938, and No. CE170100009), whose continued support created the infrastructure needed for these experiments. J. L., J. D., and K. X. wish to thank the National Natural Science Foundation of China (NSFC) Program (Grants No. 61625104 and No. 61971065), Fund of State Key Laboratory of IPOC (BUPT) (State Key Laboratory of Information Photonics and Optical Communications, Grant No. IPOC2020ZT03), and BUPT Excellent Ph.D. Students Foundation (Grant No. CX2018215) for providing the funds to purchase some specific components and to support the travel of J. L. to Australia to participate in the experiments.

*andre.luiten@adelaide.edu.au

[1] J. Zhu, S. K. Ozdemir, Y. F. Xiao, L. Li, L. He, D. R. Chen, and L. Yang, On-chip single nanoparticle detection and sizing by mode splitting in an ultrahigh-Q microresonator, Nat. Photonics **4**, 46 (2010).
[2] M. R. Foreman, J. D. Swaim, and F. Vollmer, Whispering gallery mode sensors, Adv. Opt. Photonics **7**, 168 (2015).
[3] M. D. Baaske and F. Vollmer, Optical observation of single atomic ions interacting with plasmonic nanorods in aqueous solution, Nat. Photonics **10**, 733 (2016).
[4] J. Li, M.-G. Suh, and K. Vahala, Microresonator Brillouin gyroscope, Optica **4**, 346 (2017).
[5] G. Bahl, J. Zehnpfennig, M. Tomes, and T. Carmon, Stimulated optomechanical excitation of surface acoustic waves in a microdevice, Nat. Commun. **2**, 1 (2011).
[6] G. Bahl, M. Tomes, F. Marquardt, and T. Carmon, Observation of spontaneous Brillouin cooling, Nat. Phys. **8**, 203 (2012).
[7] L. Chang, X. Jiang, S. Hua, C. Yang, J. Wen, L. Jiang, G. Li, G. Wang, and M. Xiao, Parity-time symmetry and variable optical isolation in active-passive- coupled microresonators, Nat. Photonics **8**, 524 (2014).
[8] J. Kim, M. C. Kuzyk, K. Han, H. Wang, and G. Bahl, Non-reciprocal brillouin scattering induced transparency, Nat. Phys. **11**, 275 (2015).
[9] S. M. Spillane, T. J. Kippenberg, and K. J. Vahala, Ultralow-threshold Raman laser using a spherical dielectric microcavity, Nature (London) **415**, 621 (2002).
[10] I. S. Grudinin, A. B. Matsko, and L. Maleki, Brillouin Lasing with a Caf 2 Whispering Gallery Mode Resonator, Phys. Rev. Lett. **102**, 043902 (2009).
[11] J. Li, H. Lee, and K. J. Vahala, Microwave synthesizer using an on-chip Brillouin oscillator, Nat. Commun. **4**, 1 (2013).
[12] D. Marpaung, B. Morrison, M. Pagani, R. Pant, D.-Y. Choi, B. Luther-Davies, S. J. Madden, and B. J. Eggleton, Low-power, chip-based stimulated Brillouin scattering microwave photonic filter with ultrahigh selectivity, Optica **2**, 76 (2015).
[13] M. Zhang, C. Wang, Y. Hu, A. Shams-Ansari, T. Ren, S. Fan, and M. Lončar, Electronically programmable photonic molecule, Nat. Photonics **13**, 36 (2019).
[14] L. Del Bino, J. M. Silver, S. L. Stebbings, and P. Del'Haye, Symmetry breaking of counter-propagating light in a nonlinear resonator, Sci. Rep. **7**, 43142 (2017).
[15] K. Buse, A. Adibi, and D. Psaltis, Non-volatile hologrphic storage in doubly doped lithium niobate crystals, Nature (London) **393**, 665 (1998).
[16] G. C. Valley, Evolution of phase-conjugate waves in stimulated photorefractive backscattering, J. Opt. Soc. Am. B **9**, 1440 (1992).
[17] H. Jiang, R. Luo, H. Liang, X. Chen, Y. Chen, and Q. Lin, Fast response of photorefraction in lithium niobate microresonators, Opt. Lett. **42**, 3267 (2017).
[18] A. A. Savchenkov, A. B. Matsko, D. Strekalov, V. S. Ilchenko, and L. Maleki, Enhancement of photorefraction in whispering gallery mode resonators, Phys. Rev. B **74**, 245119 (2006).
[19] A. A. Savchenkov, A. B. Matsko, D. Strekalov, V. S. Ilchenko, and L. Maleki, Photorefractive damage in whispering gallery resonators, Opt. Commun. **272**, 257 (2007).
[20] J. Wiersig, Enhancing the Sensitivity of Frequency and Energy Splitting Detection by Using Exceptional Points: Application to Microcavity Sensors for Single-Particle Detection, Phys. Rev. Lett. **112**, 203901 (2014).
[21] H. Cao and J. Wiersig, Dielectric microcavities: Model systems for wave chaos and non-hermitian physics, Rev. Mod. Phys. **87**, 61 (2015).
[22] B. Peng, Ş. K. Özdemir, F. Lei, F. Monifi, M. Gianfreda, G. L. Long, S. Fan, F. Nori, C. M. Bender, and L. Yang, Parity–time-symmetric whispering-gallery microcavities, Nat. Phys. **10**, 394 (2014).
[23] J. K. Jang, A. Klenner, X. Ji, Y. Okawachi, M. Lipson, and A. L. Gaeta, Synchronization of coupled optical microresonators, Nat. Photonics **12**, 688 (2018).
[24] R. Drever, J. L. Hall, F. Kowalski, J. Hough, G. Ford, A. Munley, and H. Ward, Laser phase and frequency stabilization using an optical resonator, Appl. Phys. B **31**, 97 (1983).

[25] M. L. Gorodetsky, A. D. Pryamikov, and V. S. Ilchenko, Rayleigh scattering in high-Q microspheres, J. Opt. Soc. Am. **17**, 1051 (2000).

[26] Z. Chen, L. Ye, J. Dai, T. Zhang, F. Yin, Y. Zhou, and K. Xu, Long-term measurement of high q optical resonators based on optical vector network analysis with Pound Drever Hall technique, Opt. Express **26**, 26888 (2018).

[27] S. Q. Fang, X. Zhang, Y. Qiao, F. R. Ling, and Y. Zhao, Fast photorefractive response in Linbo3 crystal co-doped with fe/sm ions, J. Alloys Compd. **438**, 317 (2007).

[28] T. Kippenberg, S. Spillane, and K. Vahala, Modal coupling in traveling-wave resonators, Opt. Lett. **27**, 1669 (2002).

[29] T. Erdogan, Fiber grating spectra, J. Lightwave Technol. **15**, 1277 (1997).

[30] See Supplemental Material at http://link.aps.org/supplemental/10.1103/PhysRevLett.127.033902 for a derivation of the emergence of the self-induced grating from the circulating fields, using a self-consistent, steady-state, nonlinear mode-coupling theory that accounts for charge diffusion and the optical indicatrix tensor. The Supplemental Material includes Refs. [31,32].

[31] *Photorefractive Effects and Materials*, edited by D. D. Nolte (Springer Science & Business Media, Berlin, 2013).

[32] V. I. Vinokurov and V. V. Shkunov, Theory of phase self-conjugation in unsteady stimulated backscattering in photorefractive crystals, Sov. Phys. JETP **70**, 839 (1990).

[33] X. S. Yao and L. Maleki, Optoelectronic oscillator for photonic systems, IEEE J. Quantum Electron. **32**, 1141 (1996).

[34] A. Rueda, F. Sedlmeir, M. C. Collodo, U. Vogl, B. Stiller, G. Schunk, D. V. Strekalov, C. Marquardt, J. M. Fink, O. Painter *et al.*, Efficient microwave to optical photon conversion: An electro-optical realization, Optica **3**, 597 (2016).